

# Rocket Launch Noise and the Coanda Effect

Caroline P. Lubert<sup>1</sup>, Jon N. Romero<sup>2</sup>, James S. Sochacki<sup>3</sup> and Zev C. Woodstock<sup>4</sup>  
*James Madison University, Harrisonburg, VA, 22807*

The Coanda effect is the tendency of a stream of fluid to stay attached to a convex surface, rather than follow a straight line in its original direction. Turbulent Coanda wall jets are present in a multitude of applications. The obvious advantages associated with Coanda jets compared with conventional jet flows -- in terms of substantial flow deflection, increased lift and enhanced levels of turbulence and entrainment -- are often accompanied by a considerable increase in associated noise levels and jet breakaway. Generally, the reasons for these issues are not well understood and thus the full potential offered by the Coanda effect is yet to be realized. It is clear that the ability to better predict Coanda jet noise would offer the opportunity for the Coanda principle to be more widely exploited and its potential to be more fully realized. In this paper, the results of recent modelling and experiments on a three-dimensional turbulent Coanda wall jet are presented. The application of these results to important problems of practical interest such as launch noise is also discussed, and recent data pertaining to full-scale rocket launch noise sources is presented. In particular, the behaviour of the jet exhaust within the flame trench of the Antares rocket is considered. Inside this trench a curved turbulent wall jet flows adjacent to a Coanda surface. A simple model is developed for predicting the flow in this trench and preliminary results related to the noise emitted by the rocket plume (flame) trench are discussed.

## Nomenclature

$h$	= slot width
$p_a$	= ambient pressure
$p_e$	= nozzle exit pressure
$p_0$	= pressure in the reservoir supplying the nozzle
$R_c$	= radius of Coanda flare center stem
$R_f$	= radius of spherical section of Coanda flare
$U_{jx}$	= jet exit velocity

## I. Introduction to Coanda Flows

### A. The Coanda Effect

The Coanda effect -- the phenomenon whereby "...when a jet is passed over a curved surface it bends to follow the surface, entraining large amounts of air as it does so..."<sup>1</sup> -- was first observed early in the twentieth century by Romanian mathematician and scientist Henri Coanda. In addition to occurring naturally, the Coanda principle is frequently invoked in engineering<sup>2</sup> as a result of the substantial flow deflection, enhanced levels of turbulence and increased entrainment it can offer. The significant increase in associated noise levels is an undesirable side effect which, it is suggested,<sup>3</sup> has prevented the Coanda effect from being more widely applied. The present work is part of

---

<sup>1</sup> Professor, Department of Mathematics and Statistics, MSC 1911, AIAA member

<sup>2</sup> Undergraduate Student, Department of Engineering, MSC 4113.

<sup>3</sup> Professor, Department of Mathematics and Statistics, MSC 1911.

<sup>4</sup> Undergraduate Student, Department of Mathematics and Statistics, MSC 1911.

an effort to better understand the mechanisms behind the aerodynamic noise generation of such jets, with the goal of facilitating improvements in the prediction and attenuation of such noise.

When a fluid element exits a nozzle adjacent to a curved surface, the radial equilibrium of the element leads to the development of a pressure field which forces the fluid against the surface. This effect is reinforced by the slightly enhanced viscous drag experienced by the jet on its wall side as it exits the nozzle, which also deflects it towards the surface. The pressure field continues to force the jet towards the surface, whilst an additional viscous effect -- the entrainment of the ambient fluid between the jet and the surface -- also moves the jet towards the wall. Under certain operating conditions, the entire process collapses and jet breakaway occurs, with a significant hysteresis effect.

In the case of a Coanda jet flow field, there are many complicating factors compared with plane or axisymmetric flows. These include radial expansion and streamline curvature, both of which will lead to considerably higher levels of turbulence than in the mixing layer of a plane jet. Although the growth rate of the mixing layer has been found to be similar in both cases, the potential core is generally shorter in the case of Coanda flows, because radial expansion causes the inviscid boundary layer to move towards the surface in order to conserve mass flow. It is found that the effects of source convection are much more important for a Coanda wall jet than a free jet. The shock cell structure is also found to be shorter than that of an equivalent plane jet.

The jet under consideration here is assumed to issue at high velocity from an annular exit slot. Immediately upon exit it is adjacent to a solid three-dimensional Coanda surface. The geometry of interest is shown in Fig. 1. Although this representation is that of a Coanda flare<sup>4,5</sup> of the type used in the petroleum industry (an example of which is shown in operation in Fig. 2), the experimental results and models developed herein can easily be applied to other examples of three-dimensional turbulent jet flows over Coanda surfaces.



**Figure 2. An operating Coanda flare.**

Jet flows such as that shown in Fig. 1 emit both low- and high-frequency noise. It is the latter that is of greatest interest, since it is both the most annoying to the human ear, and the easiest to attenuate. There are two primary high-frequency noise sources; turbulent mixing noise (TMN) and shock-associated noise (SAN). These will now be discussed in more detail.

### B. Turbulent Mixing Noise (TMN)

The flow field and combustion zone of the Indair flare is shown in Fig. 1. Immediately the flow leaves the nozzle exit, it entrains the ambient air, causing turbulent mixing to take place between the two. Owing to the Coanda effect, this air-gas mixture then adheres to the flare-tip surface, causing further entrainment, and turbulent shear layers are thus formed in the mixing-layer and wall-jet regions of the flare flow field. These layers play an important part in the various noise-generation mechanisms responsible for the high-frequency component of flare noise. In particular, the convection downstream of large eddies, or large-scale coherent structures present in the flare jet, by the mean jet flow, causes fluctuations in the turbulent shear stress in these shear layers. The kinetic energy of the fluctuating stress is converted to acoustic energy, and the aerodynamic noise thus generated is known as Turbulent Mixing Noise. TMN emission by turbulent Coanda jets has already been studied in some detail.<sup>6-17</sup>

### C. Shock-Associated Noise (SAN)

The turbulent Coanda flow field under investigation is two-dimensional, convergent-divergent and supersonic under most operating conditions. In contrast to subsonic jets, conditions at a downstream point in a supersonic jet cannot affect those upstream. In this way, discontinuities in flow properties can arise. Depending upon the relative pressure difference between the nozzle exit pressure ( $p_e$ ) and the ambient pressure ( $p_a$ ) a stationary shock-cell structure is present in the mixing layer region close to the jet exit slot under a wide range of operating conditions.. This effect can be seen in the

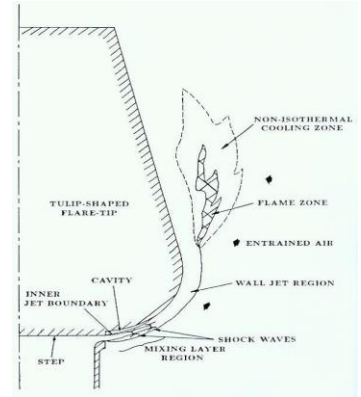


**Figure 1. The flow field and combustion zone of a Coanda flare.**

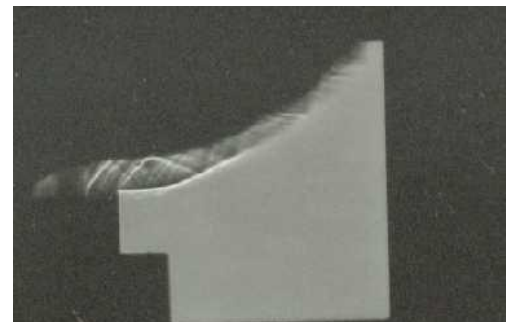


**Figure 3. Typical flow structure in Coanda flare mixing layer.**

Schlieren flow visualization photograph of Fig. 3. The exact location of these shock-waves depends upon a variety of factors including the relative magnitudes of the pressure in the reservoir supplying the nozzle ( $p_0$ ) and the pressure of the medium into which the jet flows ( $p_a$ ).

The quasi-periodic constituents of this pattern, known as shock cells, are shown schematically for a Coanda flare jet in Fig. 4. Typically a series of 8-10 shock cells will form in the jet exhaust. Turbulent eddies convected downstream within the mixing layer can successively interact with several shock waves, generating multiple sound sources (one resulting from each interaction).<sup>18</sup> This distortion of the shock front propagates away as broadband, but highly directional and strongly peaked high-frequency sound waves known as Shock-Associated Noise (SAN). Additionally, one or more feedback cycles is often present, leading to the generation of discrete, harmonically related tones.

It is well known that the flow just downstream of the jet exit slot is responsible for most of the flare noise generation and that most of the SAN is produced in this region.<sup>19</sup> Thus in order to fully comprehend this high-frequency acoustic emission, it is very important to understand the behaviour of the flow in the initial region near the nozzle exit. In particular, for the type of high speed jets presently under consideration, it is the shock-cell structure close to the slot that is of paramount importance.<sup>20</sup>

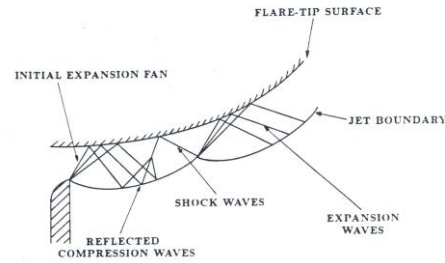


**Figure 4. Shock-cell structure near Coanda flare exit slot (reproduced from Ref. 9).**

## II. Recent Theoretical and Experimental Results

### A. Introduction

Experiments were conducted in a  $5\text{m} \times 2.5\text{m} \times 2.5\text{m}$  anechoic chamber at James Madison University. The model consisted a “tulip-shaped” body of revolution with an annular nozzle leading to an exit slot at the base of the tulip. The Coanda surface had a 53.3 mm maximum diameter, where  $R_c$  (radius of the flare center stem) = 18.056mm and  $R_f$  (radius of the spherical section of the flare) = 9mm. The jet exit velocities ( $U_{jx}$ ) were between 200m/s and 500m/s, and the exit slot ( $h$ ) varied from 1.14mm to 4.19mm. All experiments were carried out at ambient (room) temperature and pressure. Simultaneous sound measurements (using four B & K ¼ inch condenser microphones at angles of  $11.3^\circ$  (mic 1),  $5.7^\circ$  (mic 2),  $0^\circ$  (mic 3) and  $-6^\circ$  (mic 4) to the horizontal) and Schlieren flow visualization experiments were conducted. A time-synchronized digital video camera was used to record the experiments and selected frames were used to investigate flow behaviour. Shock-cells formation was observed under almost all operating conditions.

### B. Breakaway Results

Breakaway is the phenomenon that is often observed in Coanda flows when a lip shock is formed at the lower edge of the exit slot. This lip shock generates a separation bubble on the Coanda surface which grows in size with operating pressure and ultimately causes the flow to separate from the Coanda surface to which it was formerly attached.<sup>14</sup> The breakaway process is shown in more detail by the set of Schlieren photos in Fig. 5(a)-(d).

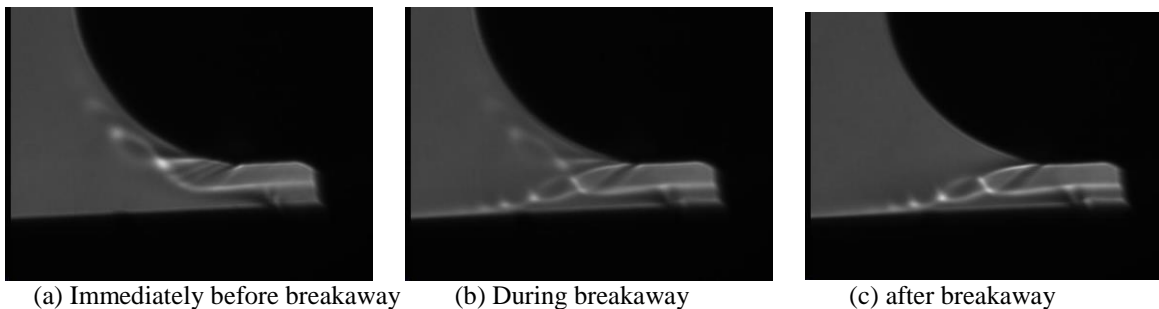


**Figure 5. Schlieren photographs showing breakaway, 2.82mm slot width.**

For the Coanda surface studied, this occurs at certain slot width-operating pressure combinations, as shown in Fig. 6. As soon as breakaway occurs, a steep drop in SPL is observed as the flow is redirected away from the horizontal. The relationship between breakaway and the observed shock cell structure and operating characteristics is currently being investigated.

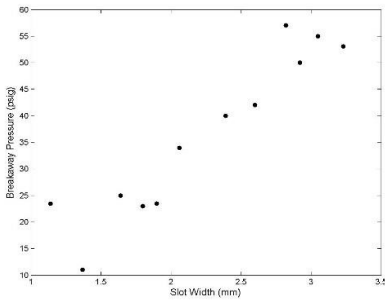


**Figure 6. Variation in breakaway pressure with slot width**

curved wall-jets than free jets. Approximate predictions have been made of some of the basic aeroacoustic properties associated with a turbulent Coanda flow. For example, the SPL has been found to approximately follow Lighthill's well-known  $U_{jx}^8$  law and  $h^2$  law. Additionally, the broadband peak frequency is found to be proportional to the maximum Coanda diameter. Accurate prediction of the acoustic source wavenumber,  $k$ , is found to be very important when modeling Coanda turbulent flows.

#### D. SAN Results

In order to facilitate prediction of SAN, the shock cell structure associated with a particular turbulent Coanda jet needs to be accurately modelled. Following Green and others<sup>13, 19,21,22</sup>, one-dimensional flow theory and the method of characteristics will be used to model flow through this nozzle. The three governing partial differential equations -- speed of sound, irrotationality and gas dynamic -- can be rewritten in terms of two non-linear ordinary differential equations; the characteristic equation and the compatibility equation. The Euler predictor-corrector numerical integration algorithm is then used to rewrite these equations as finite difference equations and solve them at points in the flare jet flow field immediately downstream of the nozzle exit. In this way, the shock cell can be estimated and compared with experimental results obtained using

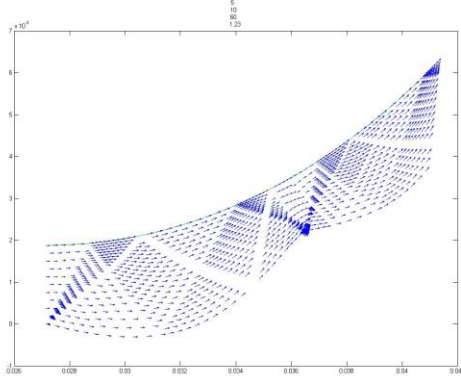


**Figure 8. Predicted Coanda jet shock cell pattern,  $U_{jx} = 467$  m/s,  $h = 3.05$ mm.**

flow visualisation techniques. Figure 8 shows the predicted shock-cell pattern for  $U_{jx} = 467$ m/s, and  $h = 3.05$ mm. Other predictions exhibit similar features. Shock waves can clearly be seen, as well as the familiar curvature of the jet boundary observed when shock cells are present. Comparison with Schlieren photographs indicates that this preliminary model of SAN is relatively accurate at predicting the location of the first shock cell formation.<sup>25</sup> Some general trends in behaviour are observed. The location of the first shock cell appears to be unaffected to any large extent by jet exit velocity, and to decrease with slot width. Breakaway is achieved under certain operating conditions and the relationship of this phenomenon to the observed shock waves is currently being investigated in more detail. The mean shock cell spacing (for the first 3-4 shock cells) appears to increase with both slot width and operating pressure. The shock cell spacing increases slightly

#### E. Coanda Jet Boundary Prediction

with distance from the nozzle. It should be noted that shock cells further from the exit slot are less well predicted, and future work will focus on modifying this preliminary model to include radial expansion and streamline curvature, which is anticipated to improve these predictions.

The sound pressure level directivity was investigated experimentally for a Coanda flow.<sup>19,23,24</sup> Figure 7 shows a typical flare spectrum. Note the presence of discrete tones in the flow. It is postulated<sup>13,14</sup> that these are generated by a self-excited acoustic feedback loop caused by the interaction between the stagnant cavity and the large-scale coherent structures in the flow. Discrete tones were generated throughout the range of operating conditions and their presence had the effect of disrupting observed trends.

#### C. TMN Results

One important result of recent work on TMN prediction<sup>3,12</sup> has been to show that the effect of source convection by jet flow is far more important in the case of

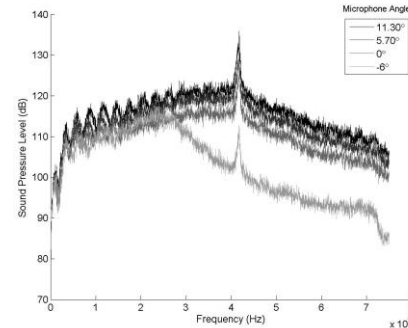


**Figure 7. Flare spectrum (54mm diameter, 2.39mm slot width, operating pressure 35 psig).**

flow visualisation techniques. Figure 8 shows the predicted shock-cell pattern for  $U_{jx} = 467$ m/s, and  $h = 3.05$ mm. Other predictions exhibit similar features. Shock waves can clearly be seen, as well as the familiar curvature of the jet boundary observed when shock cells are present. Comparison with Schlieren photographs indicates that this preliminary model of SAN is relatively accurate at predicting the location of the first shock cell formation.<sup>25</sup> Some general trends in behaviour are observed. The location of the first shock cell appears to be unaffected to any large extent by jet exit velocity, and to decrease with slot width. Breakaway is achieved under certain operating conditions and the relationship of this phenomenon to the observed shock waves is currently being investigated in more detail. The mean shock cell spacing (for the first 3-4 shock cells) appears to increase with both slot width and operating pressure. The shock cell spacing increases slightly

is influenced by jet operating characteristics. A model based on experimental data from a turbulent Coanda jet flow has recently been developed to describe the jet boundary as a function of slot width ( $h$ ) and operating pressure ( $p$ ). Shock cell location has been determined<sup>25</sup> to be extremely sensitive to the jet boundary input, and thus the impact of  $h$  and  $p$  on shock cell location is of great importance. Because of the nature of the relationship between shock cell location and breakaway, the jet boundary profile also has a previously unknown but significant impact on jet breakaway.

### III. Application to Launch Acoustics

The work described in Sections III. A - B was conducted by Panda, Mosher and Porter<sup>26</sup> on behalf of NASA and Orbital ATK. For full details of the experimental work, and other related work, please see Ref. 26. This reference also acknowledges the many other people involved in producing these results.

#### A. Introduction

During lift-off, a launch vehicle is subjected to extremely high, fluctuating acoustic loads. These loads are a principal source of structural vibration and can critically affect correct operation of the launch vehicle and its environs - the vehicle components and supporting structures. Substantial savings in unexpected repairs, operating costs and system failures can be realized by relatively small reductions in this noise level. Thus a research project was recently undertaken to identify the primary noise sources generated during the launch of the Orbital ATK Antares rocket, which currently resupplies the International Space Station (ISS). This was the first such investigation undertaken during an actual rocket launch.<sup>26</sup>

In order to identify the level and location of the various noise sources, a phased-array of 70 GRAS 1/4 inch flush-mounted condenser microphones (in a 3 m  $\times$  3 m frame) was used. The array was mounted on a scissor lift raised 12 m above the ground, at a distance of 122 m from the pad. The microphone array is shown in detail in Fig. 9.

The goal of the particular microphone layout was to maximize the array resolution at the lower frequency range (400 Hz – 2KHz) whilst also reducing the side lobes. The microphone array also housed a two-axis accelerometer and two cameras at its center (a 1.3 MPixel visible wavelength camera and a 640 pixel  $\times$  480 pixel infrared wavelength thermal camera). More details of the array, including a full description of the phased array data processing, is given by Panda, Mosher & Porter.<sup>26</sup>

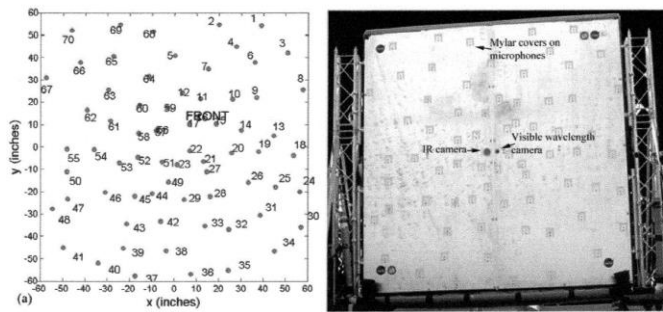


**Figure 9.(a) Microphone layout and (b) a photograph of the front surface of the 3m  $\times$  3m array. (Reproduced from Fig. 3, Ref. 26).**

Figure 10 shows the acoustic suppression system already in place on the specially-built Antares launch pad (located at Wallops Flight Facility, Wallops Island, Va) which is composed of three separate sets of water injection ports; the ‘duct inlet water’, the ‘flame trench water’ and the ‘rainbirds’ (tall and short).

The first two sources start to flow before engine ignition, whilst the rainbirds, which spray water onto the launch pad surface to prevent plume impingement damage, start at two different times, with the shorter ones starting just before the taller ones, to avoid deluging the launch vehicle.

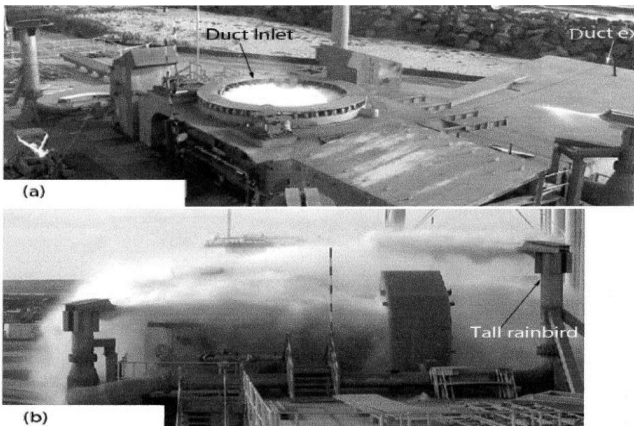


**Figure 10. Water injection systems used for acoustic attenuation in launch pad 0A. (a) Duct-inlet water; (b) on-deck ‘rainbird’ water). (Reproduced from Fig. 2, Ref. 26)**

#### B. Experimental Considerations

The microphone phased-array set-up described above was deployed at the A-One launch of the Antares rocket on April 21<sup>st</sup>, 2013. The ‘look angle’ of the cameras was determined experimentally and used to correct the results from both cameras. The rocket was sufficiently slow-moving that no Doppler-correction was necessary

in the beamforming calculations, although the delay in propagation of the sound waves from the launch pad to the face of the array needed to be accounted for.

Previous launch noise prediction models have been based on the notion of the plume as the primary noise source throughout launch. However an extremely important result of this work - which represents the first time a ground-based beamforming experiment has been conducted during an actual launch – was that the noise sources during launch were found to be time-dependent. Figure 11 clearly shows this time evolution for eight pairs of images. The left-column pictures are composites of three separate images; this is necessary to provide enough definition of the pad, which was obscured by steam, water and debris generated during launch. The three images are (a) a beamformed noise map whose levels are shown in color (b) the bottom section of a temperature map from just prior to ignition and (c) the top section of the temperature map at the time shown on the figure. The corresponding right-hand column images (selected frames from a high-speed camera) are courtesy of NASA KSC imaging group. In these figures, the Transporter Erector Launcher (TEL) can be seen releasing the launch vehicle and pitching away from the vehicle early in the launch sequence, as the launch vehicle simultaneously fires at an slight angle to the vertical away from it. This so-called ‘TEL avoidance maneuver’ significantly affects the noise distribution, because the tilting of the vehicle,

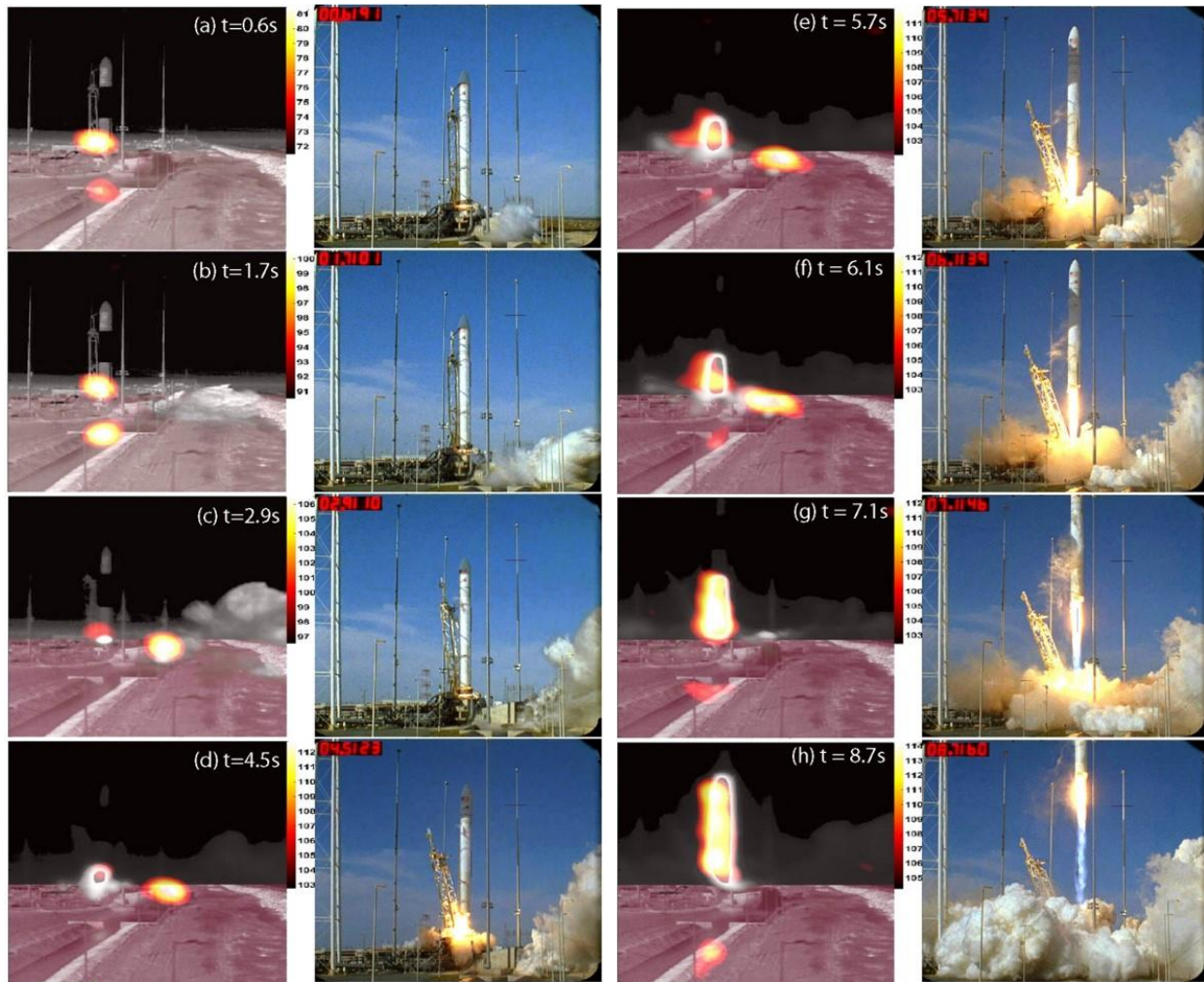


**Figure 11. Left column noise maps superimposed on frames from IR camera, conventional beamform at 2kHz; (right) corresponding frames from a high-speed camera. (Reproduced from Fig. 11, Ref. 26).**

combined with its motion, causes the hot exhaust plume (responsible for most of the noise) to spill out from the duct inlet (designed to suppress the associated noise) and spread across the launch pad. The observed start of the rainbirds (later than initially expected) compounded this problem.

Data collected from the experiments just described provided vital results not previously available. In particular, information was obtained pertaining to acoustic sources during a full-scale launch which indicated that the source distribution was very different from that used in traditional models of lift-off acoustics. These sources were found to

be time-dependent, and to depend strongly on the phase of the launch. Initially, during engine ignition (just prior to lift off) the primary noise source was the launch mount (duct inlet). However, once the engines came to full power, the hot exhaust plume exited the duct and the duct exit (J-deflector exit) became the primary source, although this effect was mitigated to some degree by the duct water. As the launch vehicle started to tilt and rise, the motion away from the duct caused the plume to spill across the launch pad and a large area on the top surface of the pad became a loud, distributed acoustic source, although initiation of the rainbirds reduced its extent. As the rocket gained vertical elevation, the plume itself became the primary noise source. At this point, the water suppression system was at full power and the rainbirds were still cooling the top of the pad, but not the plume itself, of course. Ground reflection was identified as the primary noise source only at ignition and when the plume emerged from the duct, but not in the interim.

### C. Flame Trench Modelling

A practical application of the turbulent Coanda jet flow work described previously is to launch acoustics. The experimental results discussed in the previous section indicate that a thorough understanding of the changes in

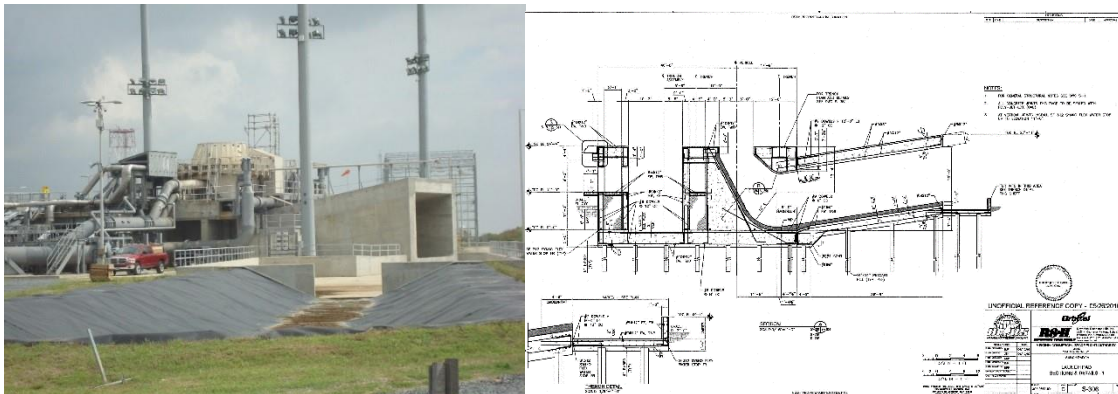


**Figure 12. (a) Photograph of J-deflector Antares rocket flame trench (J-deflector), Wallops Island, Va. (b) Technical drawing of J-deflector**

acoustic source location with launch-phase is of fundamental importance in accurately modelling launch acoustics. During this time-dependent behavior, the flame duct, or J-deflector, is a significant source of launch noise.

This flame trench, shown in Figs. 12 (a) and (b), is the primary noise source as the engines come to full power, at a time when acoustic-induced vibration is potentially very damaging to the launch vehicle and its contents. More specifically, during this period the primary noise source changes from being the duct inlet to the duct exit. Applying some of the results obtained previously (outlined in Sections II. B - E) will hopefully lead to a greater understanding of the turbulent wall jet flow within this deflector (which contains a Coanda surface at the bend, as shown in Fig. 12(b)) and might significantly contribute to noise reduction during this phase of the launch process. The benefits of reduction of acoustic load at launch have already been elucidated previously. This work is currently underway.

In order to investigate the behavior of the flow within the flame trench in more detail, a simple model was developed. Using the package Solidworks, a basic mesh was created to represent the flame duct, as shown in Fig. 13. This mesh covered the domain of interest – in this case, the flame trench (shown in the left half of Fig. 13) plus the open end of the flame trench (shown as the large area in the right half of Fig. 13). Initially this mesh comprised a number of pre-determined (by Solidworks) 3D shapes. The mesh consists of smaller elements, and each element is sufficiently small that we can assume the variables of interest, P (pressure), U (particle velocity) and T (temperature) to be homogeneous within a given element. Thus, we can approximate these values by single point values within a given element. For reasons related to computing time, the initial mesh was one element thick. Here the mesh cell size is  $0.1\text{m} \times 0.1\text{m} \times 0.1\text{m}$ , the finite mesh volume is  $813\text{m}^3$  and the final total number of cells is 81,300. OpenFOAM automatically calculated the maximum Courant number based on flow

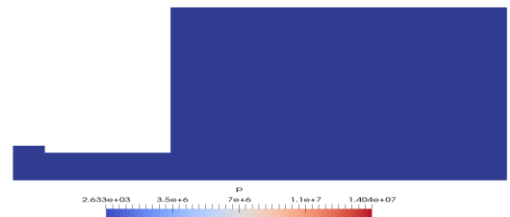


**Figure 13. Initial flame trench mesh**

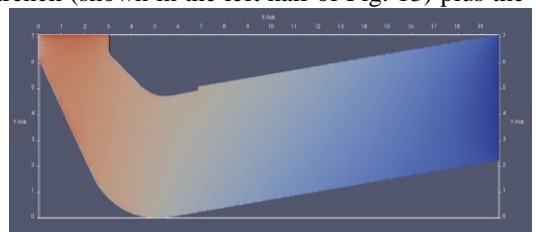


**Figure 14. Flame trench mesh with improved approximation to Coanda surface.**

velocity and error tolerance. At each timestep, the program verified that the Courant number was smaller than the maximum tolerance. Note that in this preliminary model the Coanda flow was replaced by a right angle, although in a more recent model a better approximation is made (see Fig. 14).

Once the flame trench mesh was created, the flow in the flame trench was modelled using a RAS (Reynolds-Averaged Simulation) turbulence model implemented in OpenFOAM CFD software. Initial conditions including thermodynamic conditions provided the model input for the flame trench flow field and were used to numerically

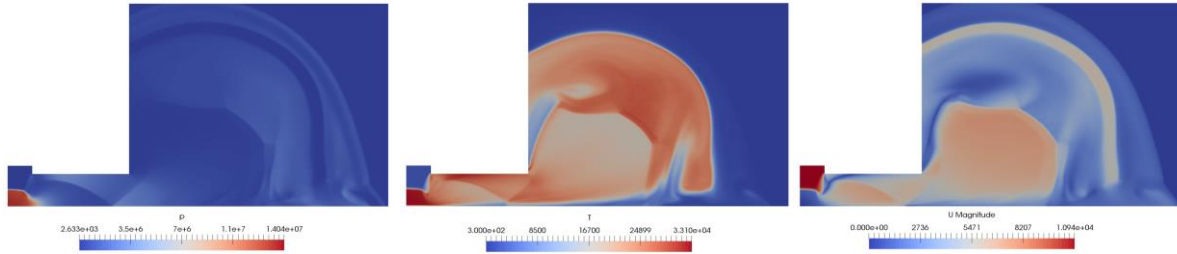


**Figure 15. (a). Pressure, P (b) Temperature, T (c) Velocity, U**  
**Results of OpenFOAM calculations at  $t = 0.0222s$**

approximate the pressure, temperature and velocity values at each of the 81,300 cells at several subsequent times. The calculations are based on the  $k-\epsilon$  model, which is the most common model used in Computational Fluid Dynamics (CFD) to simulate mean flow characteristics for turbulent flow conditions. The  $k-\epsilon$  model is a two equation model which gives a general description of turbulence by means of two transport equations. The turbulent kinetic energy,  $k$ , determines the energy in the turbulence and  $\epsilon$  represents the turbulent dissipation, which determines the rate of dissipation of the turbulent kinetic energy. The original impetus for the development of this model was to

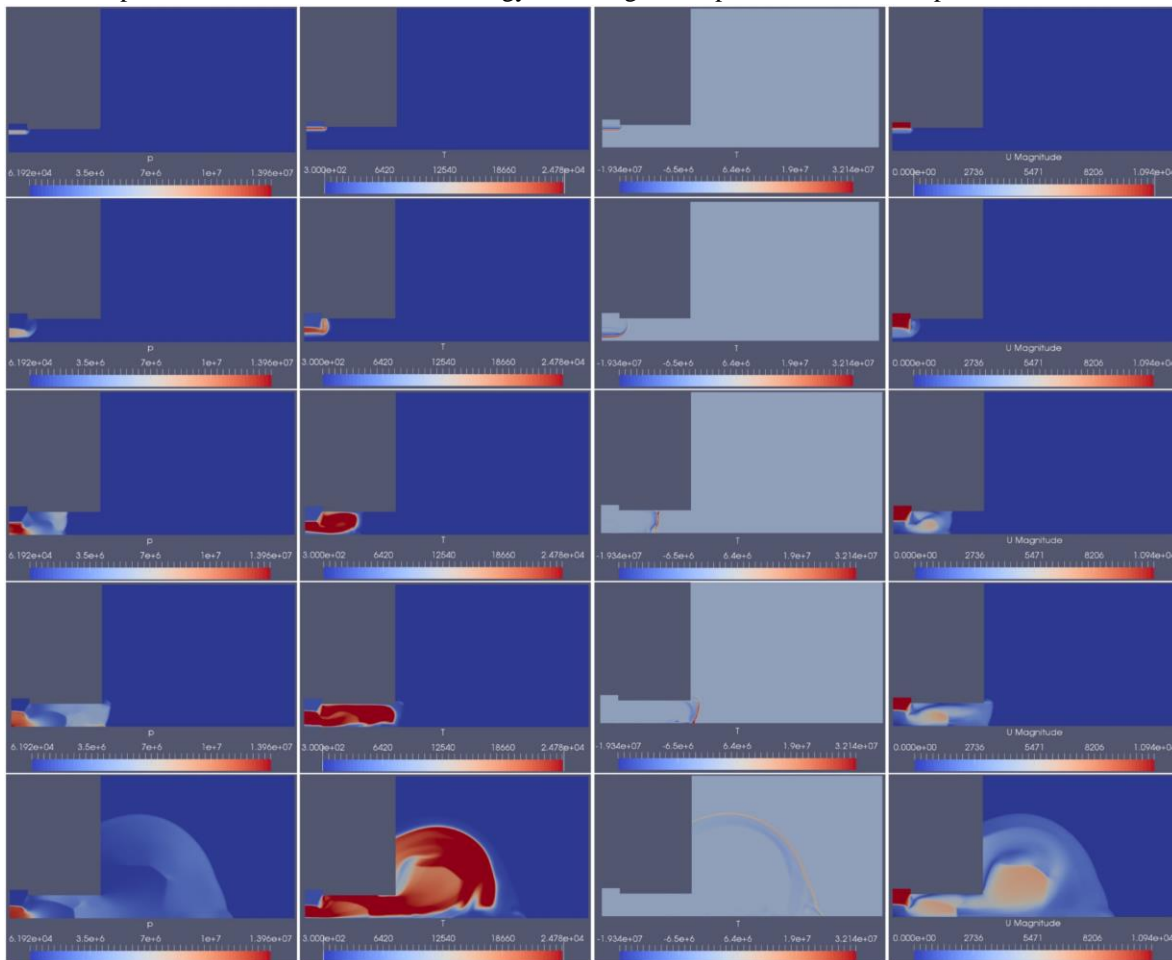


**Figure 16. (a) Pressure, P (b) Temperature, T (c) Acoustic Contours (d) Velocity, U**  
**(d) Results of OpenFOAM calculations at  $t = 0.0004s, 0.0013s, 0.0043s, 0.007s$  and  $0.0165s$  (from top to bottom)**

improve the mixing-length model, as well as to find an alternative to algebraically prescribing turbulent length scales in moderate to high complexity flows. The results of this modelling are shown in Fig. 15 (a),(b) and (d) for P, T and U at time 0.0222s

Since the solver employs a finite volume scheme (and the volume within each element in the mesh is fixed) then according to the ideal gas law, the ratio of P to T for each element in the mesh should be constant. Thus any changes (turbulence) in this constant can be assumed to correspond to acoustic turbulence, and joining lines of equal value will yield acoustic contours. Forming the ratio P/T and looking for changes using centred-difference numerical differentiation at different time steps yields the plots shown in Fig. 16(c). The corresponding values of P, T and U can be seen in Figs. 16 (a),(b) and (d). From these plots it can be seen that the only significant acoustic contours (corresponding to perturbations in the constant P/T) coincide with the front of the simulated airflow. Whilst some sections of the trench exhibited turbulence behind the air front, they only exhibited turbulence for a short period of time. Since there were no fixed locations exhibiting sustained turbulence, it was not possible to apply Lighthill's acoustic analogy and simulate the noise using (acoustic) monopoles, dipoles and quadrupoles. In future simulations, a fully three-dimensional model will be constructed in order to better capture the noise production within the flame trench.

#### IV. Summary and Conclusions

The current work has illuminated the relationship between cell location and flow characteristics, and thus the effect of jet operating conditions on SAN can now be determined. The relationship between cell location and jet breakaway is also under investigation. This work is in the process of being extended so that the Rankine-Hugoniot conditions can be used to predict the shock cell structure (and thus the SAN) along the entire jet.<sup>25</sup> Some general trends in behaviour are observed. Breakaway is achieved under certain operating conditions and the relationship of this phenomenon to the observed shock waves is currently being investigated in more detail. A comparison of these results with those of plane or axisymmetric flows highlights the difference effects that occur when dealing with Coanda wall jets.

A turbulent Coanda wall jet of current interest is the one which occurs in the flame trench used during launch of the Antares rocket. Recent experimental data has indicated that a thorough understanding of the changes in acoustic source location with launch-phase is of fundamental importance. During this time-dependent behavior, the flame trench is a fundamental player in noise generation. Specifically, it is the primary noise source when the engines reach full power, at a time when acoustic-induced vibration is potentially very damaging to the launch vehicle and its contents. A thorough understanding of this Coanda flow should contribute significantly to noise reduction during this phase of the launch process. A preliminary model of the time-dependent acoustic behavior within this trench has been developed. It is hoped that methods developed during previous work on turbulent Coanda wall jets will shortly be applied to this flow.

#### Acknowledgments

The authors wish to thank Jay Panda (NASA Ames Research Center, CA), Robert Mosher (NASA Langley Research Center, VA) and Barry Porter (Aerospace Computing, Inc., CA) as well as all at the NASA Imagery Group KSC-KX) for the use of their data and analysis pertaining to the Antares A-One launch. They also wish to thank everyone at Orbital ATK and Wallops Flight Facility for their assistance in providing access to data for this work.

#### References

- <sup>1</sup>Coanda,H., Procédé de propulsion dans un fluide, Brevet Invent. Gr. Cl. 2, no. 762688 Republique Francaise, 1932.
- <sup>2</sup>Lubert, C.P., On Some Recent Applications of the Coanda Effect, *Int. J. Acoustics and Vibration*, Vol. 16, No. 3, 2011, pp144-153.
- <sup>3</sup>Lubert, C.P, Application of Turbulent Mixing Noise Theory to Flows over Coanda Surfaces, *Int. J. Acoustics and Vibration*, Vol. 13, No. 1, 2008, pp17-30.
- <sup>4</sup>Desty, D.H. No Smoke Without Fire, *Proceedings of the Institution of Mechanical Engineers*, 197A, 1983, pp59-170.
- <sup>5</sup>Desty, D.H, Boden, J.C. and Witheridge, R.E. The Origination, Development and Application of Novel Premixed flare Burners Employing the Coanda Effect, 85th Nat. AIChE meeting, Philadelphia, 1978.
- <sup>6</sup>Lighthill, M.J., On Sound Generated Aerodynamically. I. General Theory, *Proc. Roy. Soc.*, Vol. 211, 1952, pp564-587.
- <sup>7</sup>Lilley, G.M., On the Noise from Air Jets, ARC Report 20,376, Aeronautics Research Council, UK., 1958.
- <sup>8</sup>Ribner, H.S., On the Role of Shear Noise, *J. Sound. Vib.*, Vol. 51, No. 1, 1977, pp121 – 132.
- <sup>9</sup>Parsons, C., An Experimental and Theoretical Study of the Aeroacoustics of External-Coanda Gas Flares, Ph.D. Thesis, University of Exeter, UK.,1988.
- <sup>10</sup>Smith, C., and Carpenter, P.W. The Effect of Solid Surfaces on Turbulent Jet Noise, *J. Sound and Vibration*, Vol 185, No. 3,

1995, pp397-413.

<sup>11</sup>Carpenter, P.W., and Smith, C. The Aeroacoustics and Aerodynamics of High-Speed Coanda Devices, Part 2: Effects of modifications for flow control and noise reduction, *J. Sound and Vibration*, Vol. 208, No. 5, 1997, pp803-822.

<sup>12</sup>Parsons, C., and P.W. Carpenter, The Noise Emitted by Turbulent Jets in Close Proximity to Solid Surfaces, AIAA Paper 86-1869, Proc. American Institute of Aeronautics and Astronautics, Seattle, USA., 1986.

<sup>13</sup>Carpenter, P.W., and Green, P.N., The Aeroacoustics and Aerodynamics of High-Speed Coanda Devices, Part 1: Conventional Arrangement of Exit Nozzle and Slot, *J. Sound and Vibration*, Vol. 208, No. 5, 1997, pp 777-801.

<sup>14</sup>Carpenter, P.W., and Smith, C., The Aeroacoustics and Aerodynamics of High-Speed Coanda Devices, Part 2: Effects of Modifications for Flow Control and Noise Reduction, *J. Sound and Vibration*, Vol 208, No. 5, 1997, pp 803-822.

<sup>15</sup>Curle, N., The Influence of Solid Boundaries upon Aerodynamic Sound, *Proc. Royal Soc.*, Vol. A231, 1955, pp. 505-514.

<sup>16</sup>Powell, A., Aerodynamic Noise and the Plane Boundary, *J. Acoust. Soc. America*, Vol. 32, 1960, pp982-990.

<sup>17</sup>Davies, H.G., The Radiated Fields of Multiple Point Sources near a Solid Spherical Surface, *J. Fluid Mech.*, Vol. 43, 1970, pp. 597-606.

<sup>18</sup>Harper-Bourne, M and Fisher, M.J., The Noise from Shock Waves in Supersonic Jets, Proc. AGARD Conf. on Noise Mechanisms, CP-131, Paper 11, 1973.

<sup>19</sup>Green, P.N., The Fluid Dynamics and Aeroacoustics of External Coanda Flares, PhD Thesis, University of Exeter, UK., 1987.

<sup>20</sup>Gilchrist, A.R., and Gregory Smith, D.G., Compressible Coanda Wall Jet; Predictions of Jet Structure and Comparison with Experiment, *Int. J. Heat Fluid Flow*, Vol. 9, No. 3, 1988, pp286-295.

<sup>21</sup>Carpenter, P.W. and Green, P.N. The Generation of Noise in External Coanda-Type Waste-Gas Flares, Proc. I.O.A., Vol. 6, Part 1, 1984.

<sup>22</sup>Bull, D., The Shock Associated Noise of the Indair Flare, Undergraduate project report, University of Exeter, UK., 1980.

<sup>23</sup>Morrison, J.F., A Study of an Axisymmetric Wall Jet with Streamline Curvature and its Application to the Coanda Flare, PhD Thesis, University of Durham, UK., 1982.

<sup>24</sup>Gilchrist, A.R., The Development and Breakaway of a Compressible Air Jet with Streamline Curvature and its Application to the Coanda Flare, PhD thesis, University of Durham, UK., 1985.

<sup>25</sup>Lubert, C.P., Schwantes, C. R., and Shafer, R.J., An Investigation of ShockWave Formation in Turbulent Coanda Wall Jets, *Int. J. Acoustics and Vibration*, Vol. 21, No. 2, 2016, pp199-208.

<sup>26</sup>Panda, J., Mosher, R.N., and Porter, B.J., Identification of Noise Sources during Rocket Engine Test Firings and a Rocket Launch Using a Microphone Phased-Array, NASA/TM-2013-216625, 2013.